High-quality factor optical microcavities using oxide apertured micropillars

N. G. Stoltz,[a),b)] M. Rakher,[c)] S. Strauf,[b),c)] A. Badolato,[d)] D. D. Lofgreen,[d),e)] P. M. Petroff,[b),d)] L. A. Coldren,[b),d)] and D. Bouwmeester[c)]
University of California, Santa Barbara, California 93106

(Received 28 February 2005; accepted 7 June 2005; published online 12 July 2005)

An oxide aperture is used to confine optical modes in a micropillar structure. This method overcomes the limitations due to sidewall scattering loss typical in semiconductor etched micropillars. High cavity quality factors (Q) up to 48 000 are determined by external Fabry–Perot cavity scanning measurements, a significantly higher value than prior work in III-V etched micropillars. Measured Q values and estimated mode volumes correspond to a maximum Purcell factor figure of merit value of 72. © *2005 American Institute of Physics*. [DOI: 10.1063/1.1999843]

Optical microcavities combined with active emitters provide a great opportunity to study the light-matter interaction at a fundamental level. To produce a high-quality microcavity, it is necessary to confine light to precise resonance frequencies with little or no optical loss.[1] The measure of this optical confinement is referred to as the cavity quality factor (Q). In order to limit the number of optical modes present in a cavity, it is important to reduce the effective optical mode volume (V_{eff}). Figures of merit for optical microcavity applications are proportional to the ratio of these two values Q/V_{eff}.[2] Potential applications include solid-state cavity quantum electrodynamics (CQED) experiments, modification of single-emitter lifetimes, and single-photon emitters and detectors for quantum cryptography.[1,2]

Several solid-state microcavity architectures including microdisks,[3,4] photonic crystals,[5–7] and micropillars[8,9] have shown CQED effects in III-V semiconductors using self-assembled quantum dots (QDs) as active emitters. Among these architectures, micropillars couple light normal to the semiconductor in a single-lobed Gaussian pattern that is easily fiber coupled.[10] This high photon collection efficiency makes micropillars a better alternative for device applications. However, micropillars exhibit higher $V_{\text{eff}}[\sim 5(\lambda/n)^3]$ and lower Qs($\sim$2000–10 000) when compared with photonic crystals.[1,9] V_{eff} can be reduced by decreasing pillar diameter, but scattering losses due to sidewall roughness have been shown to limit achievable Q values.[1,11]

Here, we present an alternative approach, using oxide apertured micropillars in order to reduce V_{eff} while maintaining high Q values. Oxidized micropillars have been used for vertical cavity laser applications to produce low threshold laser devices that are fabricated into inexpensive arrays for optical data networks.[12] By confining the optical mode with a laterally oxidized aperture layer these structures simultaneously provide optical mode and electrical current confinement while eliminating the scattering loss due to sidewall roughness inherent to etched pillar structures. This method has been applied to the field of QD-microcavity coupling with limited success due to very low Qs ($<$1000) as well as high $V_{\text{eff}}[\sim 35(\lambda/n)^3]$ when compared with conventional micropillars.[13,14] If these values are improved, the advantages in ease of fabrication will make oxide apertured micropillars very attractive for coupled QD-microcavity applications.

Micropillar samples investigated in this study were grown by molecular-beam epitaxy on a semi-insulating GaAs (100) substrate with a 0.1 μm buffer layer. There are four independent sections in the structure: The bottom mirror, the active region, the aperture region, and the top mirror as shown schematically in Fig. 1(a). Mirrors consist of alternating one-quarter optical thickness distributed Bragg reflector (DBR) layers of GaAs and $Al_{0.9}Ga_{0.1}As$. 32 pairs of $Al_{0.9}Ga_{0.1}As$/GaAs layers with thicknesses of 79.8/68.4 nm, respectively, form the bottom DBR mirror, while the top DBR mirror is made of 23 pairs. The active region is one optical wavelength in thickness, with two 135.4 nm layers of GaAs embedding a centered InGaAs/GaAs QD layer. QDs self-assemble during epitaxy operating in the Stranski–Krastanov growth mode. InGaAs islands are partially covered with GaAs and annealed before completely capped with GaAs. This procedure blueshifts the QDs emission wavelengths[15] toward the spectral region where Si-based de-

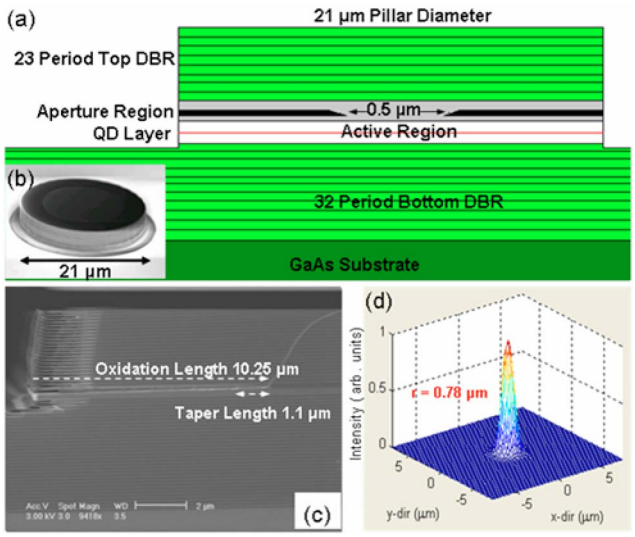

FIG. 1. (Color online) (a) Schematic and layer structure for oxide apertured micropillars. (b) SEM image of a fully processed 21 μm micropillar. (c) SEM cross section image of an oxidized mesa showing actual layer structure depicted in (a). (d) The theoretical fundamental mode profile for the 21 μm micropillar modeled in this study with a Gaussian mode radius of 0.78 μm.

[a)]Electronic mail: stoltzie@engineering.ucsb.edu
[b)]Materials Department.
[c)]Physics Department.
[d)]Electrical Engineering Department.
[e)]Currently at: Raytheon Visions Systems, Goleta, CA 93117.

tectors are more efficient. The thickness of the aperture region is three-quarters optical wavelength and consists of a pure AlAs layer sandwiched by $Al_{0.89}Ga_{0.11}As$ and $Al_{0.75}Ga_{0.25}As$ in order to produce the desired aperture qualities. It is designed to give a change in effective index, $\Delta n_{\text{eff}}=0.08$, between the fully oxidized and unoxidized regions of the micropillar in addition to a linear oxide taper with a length of 1.1 μm after an approximate 10 μm oxidation. A scanning electron microscopy (SEM) image of a fabricated oxide apertured microcavity is shown in Fig. 1(b), while Fig. 1(c) shows a cross-sectional SEM image of an oxidized mesa calibration sample with mirror, active, and aperture regions corresponding to Fig. 1(a). Samples are fabricated by optical lithography and reactive ion etch in Cl_2 plasma penetrating approximately five mirror periods into the bottom DBR. Micropillars are fabricated in large arrays with diameters varying from 21–25 μm. The wet lateral oxidation is performed at 430 °C in order to oxidize the aperture region by converting AlAs into Al_xO_y.

Microphotoluminescence (μ-PL) measurements are performed using a He-flow cryostat (4–300 K). QDs are excited nonresonantly by a continuous-wave 780 nm laser diode focused to a spot size of 2.5 μm using a microscope objective with numerical aperture of 0.55. μ-PL emission is collected through the same objective and recorded with a 1.25 m spectrometer equipped with a charge-coupled device with 30 μeV spectral resolution at 900 nm. A scanning Fabry–Perot cavity along with a single photon counting avalanche photodiode detector and an integrated counting unit are used to experimentally determine linewidths beyond the resolution of the spectrometer.

A two-dimensional model of the cavity has been developed based on the experimentally determined values for the oxide aperture taper length and core width from SEM images (Fig. 1) along with the one-dimensional reflectivity spectrum of the unprocessed sample. This produces a two-dimensional index profile determined by the effective index (n_{eff}) in the growth direction for the unoxidized and oxidized layer stack. The Δn_{eff} between the unoxidized and oxidized regions is evaluated by replacing the AlAs and $Al_{0.89}Ga_{0.11}As$ with $Al_xO_y(n=1.5)$. It has been demonstrated[16] that the linear oxide taper shown in Fig. 1(c) corresponds to a parabolic index grade over the length of the taper.

We used this model to solve for the eigenmodes of the two-dimensional scalar wave equation using a finite difference technique with a nonuniform mesh.[17] The solution for the fundamental mode of a 21 μm pillar is shown in Fig. 1(d) and has a Gaussian mode radius of approximately 0.78 μm. Scattering and radiation losses are determined by propagating a scalar field around the unfolded cavity until the field no longer changes shape. This procedure is analogous to the classic work of Fox and Li.[18]

Mirror, scattering, and radiation losses determine the empty or cold cavity linewidth of the apertured micropillar. Assuming that undoped AlGaAs regions have no internal optical loss at 4 K, the only optical loss mechanisms in the cavity are due to mirror loss (α_m), radiation loss (α_{rad}), and aperture scattering losses (α_{scat}).[17] Furthermore, α_{rad} and α_{scat} are very small for the fundamental mode, $1.7e-3$ and 1.7 cm^{-1}, respectively. This leaves photon escape through the top DBR mirror as the dominating loss mechanism in the cavity, calculated as 13.9 cm^{-1}. Cold cavity (Q_{cold}) values are determined by cavity losses according to $\omega/Q_{\text{cold}}=1/\tau_p$

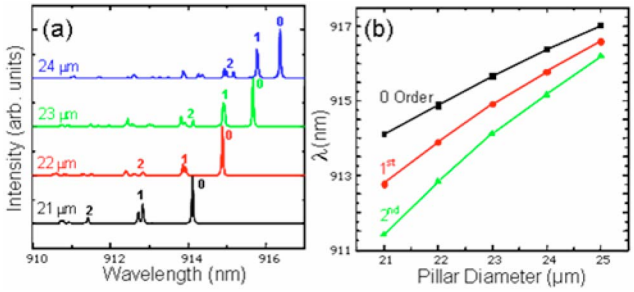

FIG. 2. (Color online) (a) Normalized optical mode spectra for 21–25 um micropillars measured by μ–PL at 4 K are shown. Fundamental, first-, and second-order modes are labeled 0, 1, and 2, respectively. (b) Mode position is shown as a function of pillar diameter for fundamental, first-, and second-order modes.

$=v_g\Gamma g_{\text{th}}=v_g(\alpha_{\text{scat}}+\alpha_{\text{rad}}+\alpha_m)$.[17] Here, τ_p is cavity lifetime, v_g is group velocity, ω is the frequency, Γ is the confinement factor, and g_{th} is the threshold material gain. The estimated Q_{cold} for a 21 μm micropillar is 14 500.

Experimental mode spectra for 21–25 μm diameter pillars are shown in Fig. 2(a) with mode orders 0, 1, and 2 labeled. The lifting of higher-order mode degeneracy is due to asymmetry in the fabrication process. μ–PL data shows cavity modes with lower fundamental energies and increasing mode spacing as pillar diameter decreases. This effect is shown in Fig. 2(b) for varying pillar diameters. In addition, intensity decreases are observed for higher-order modes due to increased scattering losses, an intentional effect produced by the oxide aperture and the larger effective radii of multilobed higher-order modes.

A Fabry–Perot scanning cavity is used to determine experimental Q values. A reference laser is used to calibrate the maximum measurable Q for the Fabry–Perot cavity as 600 000, shown in Fig. 3(a). The fundamental cavity mode is then directed through a 1 nm bandpass filter into the detector for sample measurement. Experimental quality factor (Q_{exp}) is determined to be approximately 48 000 for a 21 μm pillar as shown in Fig. 3(b). This value is larger than the theoretical

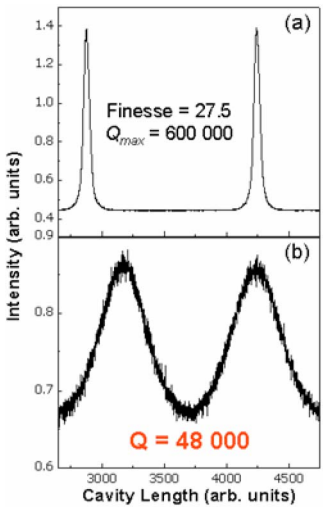

FIG. 3. (Color online) (a) Transmission through a Fabry–Perot cavity as a function of cavity length for a reference laser. Using the given free spectral range of the measurement cavity, the reference laser has $Q>600\,000$ giving a maximum measurable Q. (b) The Fabry–Perot measurement of the fundamental mode linewidth of a 21 μm micropillar cavity. This measurement was done at 50 μW pump power at 4 K.

cold cavity value due to linewidth narrowing caused by modal gain from the QD active region. The experimental gain (g_{exp}) is determined by the relationship between Q_{cold} and Q_{exp} values according to $\omega/Q_{exp}=(\omega/Q_{cold})-v_g\Gamma g_{exp}$.[17]

Q values show little change for pump powers above 10 μW and no laser threshold behavior is observed up to 50 μW pump power. This indicates that material gain in the QD layer saturates before the threshold condition is achieved. Estimated values show that g_{exp} saturates at approximately 10.44 cm^{-1}, corresponding to approximately 2864 cm^{-1} material gain from the active region. This is a reasonable value for the single QD layer in this cavity.[19] At low pump powers, Q values are expected to increase as the optically pumped QD region provides gain and causes linewidth narrowing. For the small lateral area and narrow spectral linewidths in these devices, the modal gain provided by the QD single-exciton emission saturates at pump powers below 1 μW.[6] In this regime, a slight linewidth narrowing from 0.06 to the observed 0.02 nm is expected to occur. However, it is difficult to resolve this linewidth narrowing with a scanning Fabry–Perot cavity at these low pump powers.

The Purcell factor determines the figure of merit for a coupled QD microcavity in the weak coupling regime. Using the theoretical $V_{eff}(\lambda/n_{eff})^{-3}$ of 51 and experimental Q_{exp} values, it is possible to estimate the maximum achievable F_p according to $F_p=(3/4\pi^2)(Q(\lambda/n_{eff})^3/V_{eff})$.[20] Experimentally observed values are decreased due to spectral and spatial detuning. Estimating the Purcell factor with experimental linewidths gives a maximum value of 72.

Oxidized micropillars have a promising outlook for QD-microcavity coupling due to high Q values. Further improvement for these devices could be achieved by reducing V_{eff}. Although oxide aperture micropillars reduce two-dimensional mode areas while maintaining high Q values, V_{eff} remains relatively high. This is due to the large effective cavity length in the growth direction of this structure, approximately 1.39 μm. Improvement lies in reducing this value, potentially by replacing AlGaAs/GaAs DBR mirrors with Al_xO_y/GaAs DBR mirrors having reduced mirror penetration depths.

Experimental data show very high Q (48 000) optical microcavities using an oxide apertured micropillar architecture. Devices exhibit controlled mode positions and sizes down to core widths of approximately 0.5 μm. Unlike etched air interface micropillars, which can be difficult to fabricate with acceptable loss values at smaller diameters, apertured micropillars accomplish this in a controllable and repeatable fashion. Cavities exhibit low loss values resulting from gain related linewidth narrowing effects due to stimulated emission from the QD active region. Apertured micropillars show promise for QD-microcavity coupling applications due to these high experimental Q values producing a maximum Purcell factor of 72.

This work was supported by NSF NIRT Grant No. 0304678 and DARPA Grant No. MDA 972-01-1-0027. One of the authors, S. Strauf acknowledges support from the Max-Kade Foundation.

[1] J. M. Gerard, in *Single Quantum Dots: Fundamentals, Applications, and New Concepts*, edited by P. Michler (Springer, Berlin, 2003), Vol. 90, Chap. 4, pp. 269–314.
[2] K. J. Vahala, Nature (London) **424**, 839 (2003).
[3] A. Kiraz, P. Michler, C. Becher, B. Gayral, A. Imamoglu, L. Zhang, W. V. Schoenfeld, and P. M. Petroff, Appl. Phys. Lett. **78**, 3932 (2001).
[4] E. Peter, P. Senellart, D. Martrou, A. Lemaitre, J. Bloch, J. Hours, and J. M. Gerard, available at http://xxx.lanl.gov/abs/quant-ph/0411076.
[5] T. D. Happ, I. I. Tartakovski, V. D. Kulakovskii, J.-P. Reithmaier, M. Kamp, and A. Forchel, Phys. Rev. B **66**, 041303 (2002).
[6] A. Badolato, K. Hennessy, M. Atature, J. Dreiser, E. Hu, P. M. Petroff, and A. Imamoglu, Science **308**, 1158 (2005).
[7] T. Yoshie, A. Scherer, J. Hendrickson, G. Khitrova, H. M. Gibbs, G. Rupper, C. Ell, O. B. Shchekin, and D. G. Deppe, Nature (London) **432**, 200 (2004).
[8] B. Gayral, J. M. Gérard, A. Lemaître, C. Dupuis, L. Manin, and J. L. Pelouard, Appl. Phys. Lett. **75**, 1908 (1999).
[9] J. P. Reithmaier, G. Sek, A. Loffler, C. Hofmann, S. Kuhn, S. Reitzenstein, L. V. Keldysh, V. D. Kulakovski, T. L. Reinecke, and A. Forchel, Nature (London) **432**, 197 (2004).
[10] M. Pelton, J. Vukovic, G. S. Solomon, A. Scherer, and Y. Yamamoto, IEEE J. Quantum Electron. **38**, 170 (2002).
[11] T. Rivera, J.–P. Debray, J. M. Gerard, B. Legrand, L. Manin-Ferlazzo, and J. L. Oudar, Appl. Phys. Lett. **74**, 911 (1999).
[12] L. A. Coldren, H. Temkin, and C. W. Wilmsen, *Vertical-Cavity Surface-Emitting Lasers*, 1st ed. (Cambridge University Press, Cambridge, UK, 1999), Vol. 1, Chap. 1 , p.1.
[13] L. A. Graham, D. L. Huffaker, and D. G. Deppe, Appl. Phys. Lett. **74**, 2408 (1999).
[14] D. G. Deppe, L. A. Graham, and D. L. Huffaker, IEEE J. Quantum Electron. **35**, 1502 (1999).
[15] P. M. Petroff, A. Lorke, and A. Imamoglu, Phys. Today **54**, 46 (2001).
[16] E. R. Hegblom, N. M. Margalit, A. Fiore, and L. A. Coldren, IEEE J. Sel. Top. Quantum Electron. **5**, 553 (1999).
[17] L. A. Coldren and S. W. Corzine, in *Diode Lasers and Photonic Integrated Circuits*, 1st ed. edited by K. Chang (Wiley, New York, 1995), Vol. 1, Chap. 16 Apps. 4,16, pp.188, 226, 444, 563–567.
[18] A. G. Fox and T. Li, Bell Syst. Tech. J. **40**, 453 (1961).
[19] S. Schneider, P. Borri, W. Langbein, U. Woggon, R. L. Sellin, D. Ouyang, and D. Bimberg, IEEE J. Quantum Electron. **40**, 1423 (2004).
[20] E. M. Purcell, Phys. Rev. **69**, 681 (1946).